Available online at www.sciencedirect.com

ScienceDirect

IFAC PapersOnline CONFERENCE PAPER ARCHIVE

IFAC PapersOnLine 51-1 (2018) 456–461

A Novel Bi-rotor Configuration and its Control

Kedarisetty Siddhardha *

* *K. Siddhardha is with Department Aerospace Engineering, IIT Madras, Chennai, India (e-mail: siddhardhak2010@gmail.com).*

Abstract: A novel bi-rotor configuration that uses reaction wheels to control the system attitude (roll and yaw) is presented in this article. This configuration exploits the fact that moment of inertia about the axis connection the two rotors (roll axis) is significantly less compared to moment of inertia about the other two orthogonal axes (pitch and yaw axes). A detailed mathematical model of the proposed configuration is presented. PD controllers are used to control the attitude and position of the system. Particle swarm optimization is used to obtain the controller gains and also to infer the role of actuator dynamics on system performance. The simulation results for attitude, position command tracking and way-point trajectory tracking are shown to demonstrate the performance of the proposed configuration.

Keywords: Reduced gravity, quadrotor, autonomous control, system modelling.

1. INTRODUCTION

In the last two decades, development and use of unmanned aerial vehicles (UAVs) received abundant interest from military, academic and industrial sectors Bouabdallah (2004)-Santana (2015). Among the various UAV configurations, multi-rotors emerged as one of the most popular UAV platforms owing to its vertical take off landing (VTOL) and hover capabilities. These platforms are extensively used for military and civilian applications such as tactical support, surveillance, traffic monitoring, cinematography, sports coverage, disaster response and medical assistance Gupte (2012).

Although quad-rotor was, and remained, the center of attraction among multi-rotor platforms, other multi-rotor platforms such as bi-rotors, tri-rotors, hex-rotors etc., are also developed and studied Escareno (2006)-Christian (2014), Kulhare (2012). Multi-rotor platforms with more than four rotors are more reliable in case of motor failures owing to the actuator redundancy they possess. Whereas, multi-rotors with less than four rotors are preferred when high efficiency (less power consumption) is desired, as it is known that a large single rotor is more efficient than multiple small rotors with equal net rotor areas Scott (2013). Thus, bi-rotors are more efficient compared to other multi-rotor platforms. However, as a bi-rotor is under actuated, other actuation mechanisms or devices such as tilt-rotors or wake deflection wanes are necessary to stabilize and control the attitude of bi-rotors Escareno (2006)-Christian (2014).

There haven't been many advances in design and control of bi-rotor. Few available works in the literature are referred here. One way to control the attitude of a bi-rotor is via a tilt rotor mechanism which allows the rotors to be tilted about the axis connecting the two rotors Escareno (2006), Goncalves (2013). By providing the rotors with more than one degree of tilting, the attitude subsystem can be made over-actuated Farid (2006). Another way of controlling bi-rotors with tilt rotor mechanism is by harnessing the pitching moment caused because of gyroscopic effects due to rotor angular momentum and tilt rate of rotors. This mechanism is known as oblique active tilting (OAT) Christian (2014). In Gress (2007), a bi-rotor that can be converted to a VTOL aircraft is proposed that can stabilize hover with the help of wake deflection using elevators and ailerons. In this paper, we propose a novel bi-rotor configuration, referred to as BiRW hereafter, that uses reaction wheels (RW) to control roll and yaw degrees of freedom. The reaction wheels are controlled by DC motors. The counter torque produced by the DC motor-RW combination is used to control roll and yaw of BiRW. Pitch of this bi-rotor is controlled using the moment generated due to the thrust difference between the two rotors. BiRW configuration exploits the fact that the moment of inertia about roll axis is significantly less compared to yaw and pitch axes and therefore a small RW would suffice to control roll. We present a detailed mathematical model of BiRW. We propose to use standard PD control laws, gains of which are obtained using particle swarm optimization (PSO) by minimizing the deviation of the system performance and stability from desired time domain and frequency domain specifications. The performance of BiRW with designed controller is demonstrated in simulations through attitude command tracking and way-points trajectory tracking.

2. BIRW CONFIGURATION

A schematic of the proposed bi-rotor configuration (BiRW) is shown in Fig. 1. BiRW actuators consists of two brushless DC (BLDC) motors and two DC motors. BLDC motor-propeller combinations produce thrust and pitching moment. Cumulative thrust of the two BLDC motor-propeller combinations is attributed to total thrust produced by BiRW, whereas differential thrust of this combination results in pitching moment.

10.1016/j.ifacol.2018.05.076

Each DC motor drives a reaction wheel. The counter torque produced by DC motor-RW combination produces rolling and yawing moments. DC motors and RWs are chosen such that the counter torques produced by them are sufficient to control yaw and roll of BiRW. The simplest solution to control roll and yaw using RWs would be to place each DC motor-RW combination along each of roll and yaw axes. Since the moment of inertia about yaw axis is much larger than moment of inertia about roll axis, to attain similar control effectiveness, the DC motor-RW along yaw axis would be required to be far larger in size. Instead, for our configuration, we choose two identical DC motors and RWs. To attain similar control effectiveness, we position DC motor-RW combinations at an angle with respect to roll axis (refer to Fig.2) such that ratio of the combined maximum counter torque components about roll and yaw axes is equal to the ratio of moment of inertia of the BiRW about these axes.

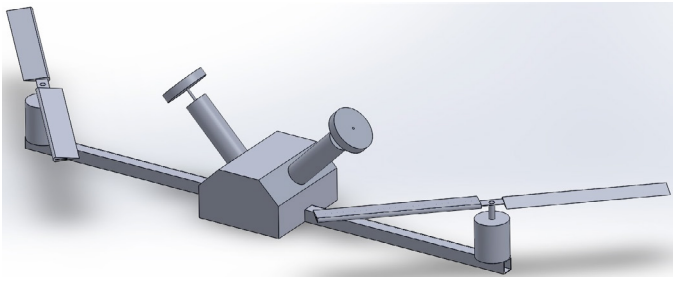

Fig. 1. BiRW configuration

3. MATHEMATICAL MODEL

In this section, we model the actuators of BiRW, the forces and moments acting on the bi-rotor, and derive the equations governing the motion of BiRW. Definitions of various parameters that appear in the modeling and the numerical values used in simulations presented in this paper are given in the appendix. The reader may refer to the tables in the appendix for explanation of the symbols used in the equations that follows.

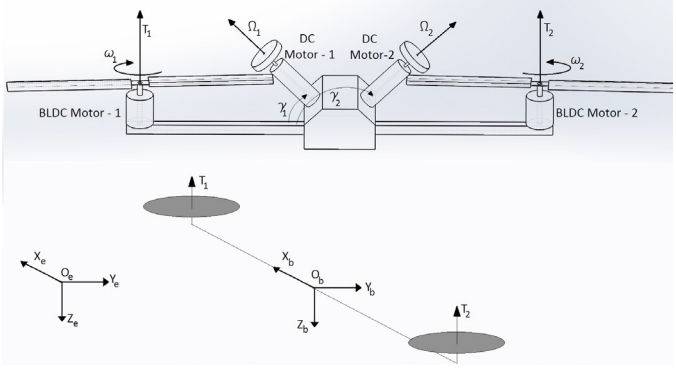

Fig. 2. BiRW description and reference frames

3.1 Reference frames

We choose a body fixed frame x_b-y_b-z_b as shown in Fig. 2. Its origin 'O_b' coincides with the center of gravity of BiRW. The unit vectors along positive x_b, y_b and z_b directions are $\boldsymbol{i}_b$, $\boldsymbol{j}_b$ and $\boldsymbol{k}_b$ respectively. Inertial reference frame is chosen as the Earth fixed frame x_e-y_e-z_e which is the standard North-East-Down frame as shown in Fig. 2.

3.2 Modeling of actuators

The actuation mechanism of BiRW comprise DC motors and BLDC motors.

DC motor In our modeling, DC motors are assumed to have viscous as well as Coulomb friction (a constant torque opposing rotation). The mathematical model for a DC motor is given by the following set of equations.

$$\frac{\mathrm{d}i_a}{\mathrm{d}t} = -\frac{R_a}{L_a}i_a - \frac{k_b}{L_a}\Omega + \frac{1}{L_a}e_a,\ \frac{\mathrm{d}\Omega}{\mathrm{d}t} = \frac{k_t}{J}i_a - \frac{B}{J}\Omega - \frac{f}{J}\mathrm{sgn}(\Omega) \tag{1}$$

where e_a is the applied armature voltage.

BLDC motor An accurate mathematical modeling of BLDC motor is much more complicated compared to DC motor modeling owing to its complex construction. Therefore, an approximate mathematical model for BLDC motor is given as

$$\frac{\mathrm{d}\omega}{\mathrm{d}t} = -\frac{1}{\tau_m}\omega + \frac{k_d}{\tau_m}e \tag{2}$$

where, ω is shaft angular speed of BLDC motor and e is the voltage supplied to integrated switching circuit.

3.3 Modeling forces

We assume that drag force acting on the body is negligible, therefore, we consider only gravitational force and the thrust produced by rotors.

Table 1. BiRW forces

Description	Definition
Force due to gravity ($\boldsymbol{F_g}$)	$-mg\sin\theta\boldsymbol{i}_b + mg\sin\phi\cos\theta\boldsymbol{j}_b + mg\cos\phi\cos\theta\boldsymbol{k}_b$
Force produced by rotors ($\boldsymbol{F_p}$)	$-b\sum_{i=1}^{2}\omega_i^2\boldsymbol{k}_b$

where ϕ, θ and ψ are roll, pitch and yaw Euler angles respectively that describe the attitude of BiRW in inertial frame of reference and g is the acceleration due to gravity.

3.4 Modeling moments

BiRW experiences moment due to counter torques and gyroscopic effects. These are modeled as follows

Table 2. BiRW moments

Description	Definition
Propeller torque ($\boldsymbol{\tau_d}$)	$(T_1 - T_2)l\boldsymbol{j}_b + \sum_{i=1}^{2}Q_i\boldsymbol{k}_b$
Reaction wheel counter torque ($\boldsymbol{\tau_r}$)	$J\sum_{i=1}^{2}\left[-\frac{\mathrm{d}\Omega_i}{\mathrm{d}t}\cos\gamma_i\boldsymbol{i}_b + \frac{\mathrm{d}\Omega_i}{\mathrm{d}t}\sin\gamma_i\boldsymbol{k}_b\right]$
Body gyroscopic torque ($\boldsymbol{\tau_{gm}}$)	$J_m\sum_{i=1}^{2}(-1)^i\omega_i\left[-q\boldsymbol{i}_b + p\boldsymbol{j}_b\right]$
RW gyroscopic torque ($\boldsymbol{\tau_{gr}}$)	$J\sum_{i=1}^{2}\Omega_i\left[-q\sin\gamma_i\boldsymbol{i}_b + (p\sin\gamma_i + r\cos\gamma_i)\boldsymbol{j}_b - q\cos\gamma_i\boldsymbol{k}_b\right]$

where, p, q and r are body rates along x_b, y_b and z_b respectively. The thrust and counter torque by i^{th} propeller are $T_i = b{\omega_i}^2$, $Q_i = (-1)^i d{\omega_i}^2$, $\quad i = 1, 2$.

3.5 Governing equations

The translation and attitude governing equations of BiRW are given by the standard Newton-Euler rigid body equations

$$\frac{\mathrm{d}(m\boldsymbol{V_b})}{\mathrm{d}t} + \boldsymbol{\Omega}_\mathrm{b} \times (m\boldsymbol{V}_\mathrm{b}) = \boldsymbol{F}_\mathrm{b}, \frac{\mathrm{d}(\boldsymbol{I\Omega}_\mathrm{b})}{\mathrm{d}t} + \boldsymbol{\Omega}_\mathrm{b} \times (\boldsymbol{I\Omega}_\mathrm{b}) = \boldsymbol{\tau}_\mathrm{b} \tag{3}$$

where, $\boldsymbol{V}_\mathrm{b} = u\,\boldsymbol{i}_\mathrm{b} + v\,\boldsymbol{j}_\mathrm{b} + w\,\boldsymbol{k}_\mathrm{b}$, $\boldsymbol{\Omega_b} = p\,\boldsymbol{i}_\mathrm{b} + q\,\boldsymbol{j}_\mathrm{b} + r\,\boldsymbol{k}_\mathrm{b}$, $\boldsymbol{F}_\mathrm{b} = \boldsymbol{F}_g + \boldsymbol{F}_\mathrm{p}$, and $\boldsymbol{\tau}_\mathrm{b} = \boldsymbol{\tau}_\mathrm{d} + \boldsymbol{\tau}_\mathrm{r} + \boldsymbol{\tau}_\mathrm{gm} + \boldsymbol{\tau}_\mathrm{gr}$.

The forces and moments are modeled in body frame of reference, where as the position (x, y, z) and attitude commands to BiRW are provided in Earth frame. Thus, we use standard Euler angle representation (ϕ, θ, ψ).

4. CONTROL OF BIRW

4.1 System architecture

Translation, attitude and propulsion are coupled in a BiRW. The attitude of BiRW is controlled by counter torques of DC motors and thrust difference between the rotors. Translation motion is controlled by varying its attitude and thrust. Thus, BiRW has a cascaded architecture. The translation, attitude and propulsion subsystems are pictorially represented in Fig. 3.

The translation controller provides desired attitude as input to attitude controller. The attitude and translation controller commands the actuators via desired pseudo inputs as shown in Fig. 3. The output of the actuator subsystem are pseudo inputs (actual) to attitude and translation dynamics.

By linearizing and applying Laplace transform to (3) and substituting the actuator dynamics, we obtain the attitude and altitude governing equations in frequency domain as shown below.

$$\begin{aligned}
\Delta\phi(s) &= \frac{\left(\frac{-Jk_\mathrm{t}}{I_\mathrm{x}JL_\mathrm{a}}\right)(-e_{\mathrm{a}_1}\cos\gamma_1 - e_{\mathrm{a}_2}\cos\gamma_2)}{s^3 + \left(\frac{JR_\mathrm{a}+L_\mathrm{a}B}{JL_\mathrm{a}}\right)s^2 + \left(\frac{BR_\mathrm{a}+k_\mathrm{t}k_\mathrm{b}}{JL_\mathrm{a}}\right)s} \\
\Delta\theta(s) &= \frac{2b\omega_0 l k_\mathrm{d}(e_1 - e_2)}{\tau_\mathrm{m} I_\mathrm{y} s^3 + I_\mathrm{y} s^2} \\
\Delta\psi(s) &= \frac{\left(\frac{-Jk_\mathrm{t}}{I_\mathrm{z}JL_\mathrm{a}}\right)(e_{\mathrm{a}_1}\sin\gamma_1 + e_{\mathrm{a}_2}\sin\gamma_2)}{s^3 + \left(\frac{JR_\mathrm{a}+L_\mathrm{a}B}{JL_\mathrm{a}}\right)s^2 + \left(\frac{BR_\mathrm{a}+k_\mathrm{t}k_\mathrm{b}}{JL_\mathrm{a}}\right)s} \\
\Delta z(s) &= -\frac{2b\omega_0 l k_\mathrm{d}(e_1 + e_2)}{\tau_\mathrm{m} s^3 + s^2}
\end{aligned} \tag{4}$$

From (4), we can define the desired pseudo inputs as

$$\begin{bmatrix} u_{1\mathrm{d}} \\ u_{2\mathrm{d}} \\ u_{3\mathrm{d}} \\ u_{4\mathrm{d}} \end{bmatrix} = \begin{bmatrix} 0 & 0 & -\cos\gamma_1 & -\cos\gamma_2 \\ 1 & -1 & 0 & 0 \\ 0 & 0 & \sin\gamma_1 & \sin\gamma_2 \\ 1 & 1 & 0 & 0 \end{bmatrix} \begin{bmatrix} e_1 \\ e_2 \\ e_{\mathrm{a}_1} \\ e_{\mathrm{a}_2} \end{bmatrix} \tag{5}$$

where, $u_{1\mathrm{d}}$, $u_{2\mathrm{d}}$,$u_{3\mathrm{d}}$ and $u_{4\mathrm{d}}$ are desired roll, desired pitch, desired yaw and desired thrust pseudo inputs respectively to actuator subsystem. The desired pseudo inputs $u_{1\mathrm{d}}$, $u_{2\mathrm{d}}$ and $u_{3\mathrm{d}}$ are provided to actuator subsystem by attitude controller. Whereas, $u_{4\mathrm{d}}$ (also referred to as T_d) is provided to actuator subsystem by translation controller. We choose PD controllers to stabilize and control attitude and translation motion of BiRW.

4.2 Attitude and position control

Attitude control The control laws corresponding to roll, pitch and yaw degrees of freedom are

$$\begin{aligned}
u_{1\mathrm{d}} = k_{\mathrm{p}_\phi} e_\phi + k_{\mathrm{d}_\phi}\frac{\mathrm{d}e_\phi}{\mathrm{d}t}, u_{2\mathrm{d}} = k_{\mathrm{p}_\theta} e_\theta + k_{\mathrm{d}_\theta}\frac{\mathrm{d}e_\theta}{\mathrm{d}t}, \\
u_{3\mathrm{d}} = k_{\mathrm{p}_\psi} e_\psi + k_{\mathrm{d}_\psi}\frac{\mathrm{d}e_\psi}{\mathrm{d}t}
\end{aligned} \tag{6}$$

where, e_ϕ, e_θ and e_ψ are attitude errors that is the deviation of actual from desired attitude.

Position control The translation controller commands the attitude subsystem by demanding required roll and pitch angles. Whereas, the desired yaw angle is always zero. Thus, BiRW spatial movement is produced by rolling, pitching and varying the thrust of rotors. The control laws corresponding to position are

$$\begin{aligned}
\theta_\mathrm{d} = k_{\mathrm{p}_\mathrm{x}} e_x + k_{\mathrm{d}_\mathrm{x}}\frac{\mathrm{d}e_x}{\mathrm{d}t}, \phi_\mathrm{d} = k_{\mathrm{p}_\mathrm{y}} e_y + k_{\mathrm{d}_\mathrm{y}}\frac{\mathrm{d}e_y}{\mathrm{d}t} \\
T_\mathrm{d} = k_{\mathrm{p}_\mathrm{z}} e_z + k_{\mathrm{d}_\mathrm{z}}\frac{\mathrm{d}e_z}{\mathrm{d}t}
\end{aligned} \tag{7}$$

where θ_d, ϕ_d, T_d are desired pitch, roll and thrust respectively. In the above equations, e_x, e_y and e_z are translation errors.

The proportional and derivative gains of the above control laws decide the stability and performance of BiRW. Thus, it is important to choose the control gains that satisfy the user specifications. The control law design will be performed in the following subsection.

4.3 Control law design algorithm

Designing PD controllers as described above amounts to choosing appropriate values of tuning parameters k_p and k_d. The choice of (k_p, k_d) should provide desired stability and performance. The desired stability is specified through gain and phase margins. Time domain specifications are considered as measure for desired system performance. Desired time domain and frequency domain specifications for translation and attitude subsystems are given in Table 3. The desired specifications are chosen such that the attitude subsystem being the inner loop should be faster compared to the translation subsystem. In order to choose the appropriate tuning parameters that

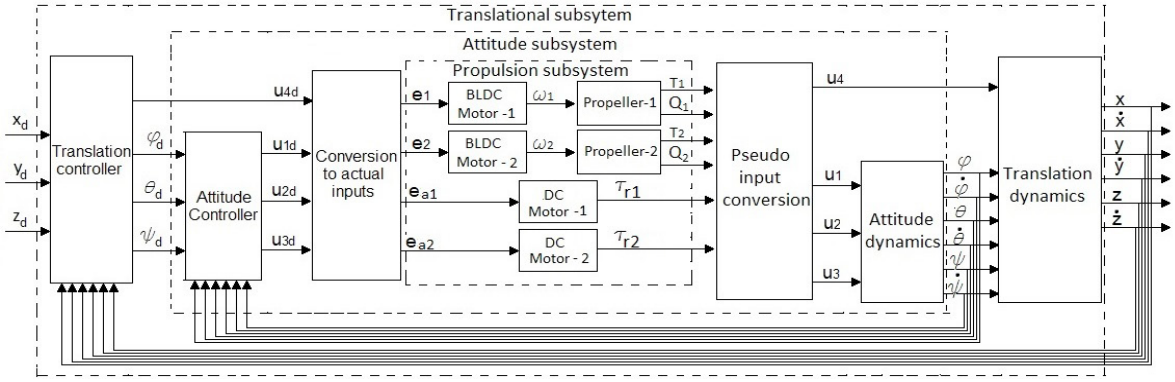

Fig. 3. BiRW system architecture

will result in a controller satisfying desired specifications, one can perform a brute force search over the k_p - k_d plane. To save computational effort, we employ PSO.

PSO is a meta heuristic optimization technique that optimizes a cost function through an iterative process. It starts with a set of particles (solution candidates) scattered in the search domain. Each particle has a cost associated with it which is equal to the value of the cost function evaluated at that point in the search domain where the particle is. During every iteration step, the particles move in the search domain according to some law that takes into account the current cost of the particles and the best cost that a particle has encountered in previous iterations. Such a law usually gives a probabilistic guarantee that after sufficient number of iterations, all the particles will converge to a single point which also will be the global minimum of the cost function Yuhui (1998).

Table 3. Desired specifications

Specification	Attitude	Translation
Overshoot (o_{s_d})	0	0
Undershoot (u_{s_d})	0	0
Settling time (t_{s_d})	0.6 sec	3 sec
Rise time (t_{r_d})	0.3 sec	1.5 sec
Gain margin (G_d)	$\geq$ 8 dB	$\geq$ 6 dB
Phase margin (P_d)	$\geq$ 60°	$\geq$ 40°

We use PSO algorithm to select tuning parameters for PD controllers for all degrees of freedom.The cost function used is one that will minimize the difference between achieved and desired performance.

$$\Gamma = \left(u_s - u_{s_d}\right)^2 + \left(o_s - o_{s_d}\right)^2 + \left(t_s - t_{s_d}\right)^2 + \left(r_s - r_{s_d}\right)^2 + \left(G_d - \min(G, G_d)\right)^2 + \left(P_d - \min(P, P_d)\right)^2 \quad (8)$$

PSO Algorithm The PSO algorithm employed is given in Algorithm 1. In order to increase the probability of achieving global minimum, once the convergence is achieved, we store the optimal control gains to which the particles converged and scatter the particles to repeat the optimization process. Such process of scattering is done $lScatter$ times. In the end, we consider the minimum cost of all the scatter iterations.

PSO Results Convergence plot of PSO iterations for roll controller is shown in Fig. 4. The gain values and corresponding cost for roll and pitch controllers are shown in Table 4.

Algorithm 1 PSO algorithm

Input: Desired specifications, Open loop transfer function
Output: Gains with least cost for every scatter iteration
procedure
  for k = 1 to lScatter **do**
    Initialize $nParticle$ particles with random locations on k_p - k_d plane within the given bounds.
    for j = 1 to mIteration **do**
      for i = 1 to nParticle **do**
        Evaluate close loop transfer function using the particle location $\left(k_p(i), k_d(i)\right)$.
        Calculate o_s, u_s, t_s, t_r, G and P from closed loop transfer function.
        Evaluate $\Gamma(i)$ using (37).
        $[l_p(i), l_d(i)] \longleftarrow \text{argmin}\left(\text{lMin}(i), \Gamma(i)\right)$
        $\text{lMin}(i) \longleftarrow \min\left(\text{lMin}(i), \Gamma(i)\right)$
        $k_p(i) = c_1\left(l_p(i) - k_p(i)\right) + c_2\left(g_p - k_p(i)\right) + k_p(i)$
        $k_d(i) = c_1\left(l_d(i) - k_d(i)\right) + c_2\left(g_d - k_d(i)\right) + k_d(i)$
      end for
      $[g_p, g_d] \longleftarrow \text{argmin}\left(\text{gMin}, \min(\Gamma)\right)$
      $\text{gMin} \longleftarrow \min\left(\text{gMin}, \min(\Gamma)\right)$
    end for
    return $[g_p, g_d, \text{gMin}]$ as k^{th} scatter iteration result
  end for
end procedure

The Table 5 shows us the optimal control gains obtained from PSO algorithm for all degrees of freedom. The cost for roll degree of freedom is comparatively much lower than pitch because the desired performance in terms of rise time and settling time could not be achieved. This is because the actuator (BLDC motor) that controls the pitch has lower bandwidth compared to actuator (DC motor) that controls the roll. The reason for such choice of actuators is explained in detail in attitude and translation control simulation results.

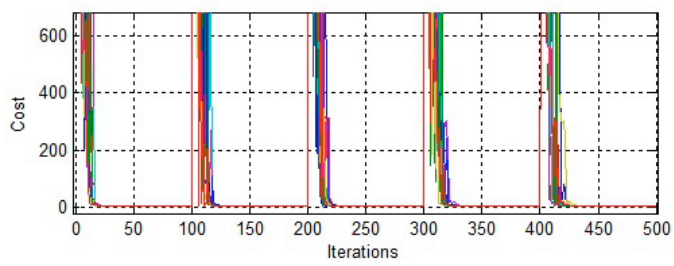

Fig. 4. Scatter - convergence of particles

Table 4. Roll and pitch controller gains and cost from PSO

Scatter iteration	Roll gains (k_{p_ϕ}, k_{d_ϕ})	Cost	Pitch control gains $(k_{p_\theta}, k_{d_\theta})$	Cost
1	(-44.9, -91.6)	0.4486	(0.93e-5, 0.0575)	6.6319
2	(-44.9, -91.6)	0.4486	(0.47e-5, 0.0550)	6.5154
3	(-32.1, -0.27)	0.61e-3	(0.47e-5, 0.0550)	6.5154
4	(-32.1, -0.27)	0.61e-3	(0.47e-5, 0.0550)	6.5154
5	(-32.1, -0.27)	0.61e-3	(0.47e-5, 0.0550)	6.5154

Table 5. Optimal control gains from PSO algorithm

Control gains	Value
(k_{p_ϕ}, k_{d_ϕ})	(-32.1, -0.271)
$(k_{p_\theta}, k_{d_\theta})$	(0.47e-5, 0.0550)
(k_{p_ψ}, k_{d_ψ})	(-230.67, -2.02)
(k_{p_x}, k_{d_x})	(-0.04, -0.105)
(k_{p_y}, k_{d_y})	(0.67, 0.4708)
(k_{p_z}, k_{d_z})	(-0.8100, -1.6200)

The reason for which negative values of control gains obtained from PSO algorithm in Table 5 is purely due to the choice of convention of reference frames. The simulation results for attitude command tracking and position command tracking using the optimal control gains shown in Table 5 is shown in the subsequent subsection.

4.4 Simulation results

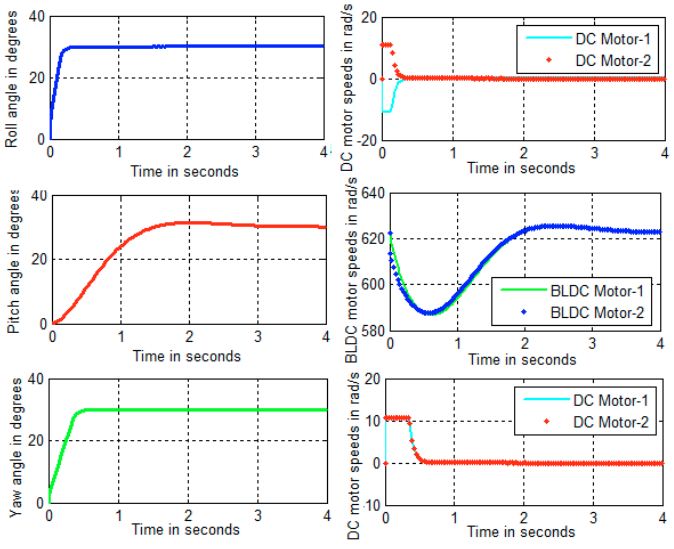

Fig. 5. Attitude control

Attitude control BiRW attitude control simulation results along with actuator inputs are shown in Fig. 5. We can observe from the plots in Fig. 5, that the roll and yaw responses obtained are comparatively faster than pitch response despite the fact that the desired specifications are same. This is due to difference in actuator time constants. The DC motors chosen are much faster compared to BLDC motors. In order to have faster pitch response, we need to choose BLDC motor of higher bandwidth. However, BLDC motors with high bandwidth cannot provide high torque. BLDC motors with high torque requirements needs to be larger in size (more number of coils), thus larger the rotor inertia and slow speed response (low bandwidth). Thus, the maximum speed at which the high bandwidth motors can rotate with propellers on will reduce, leading to low thrust capabilities.

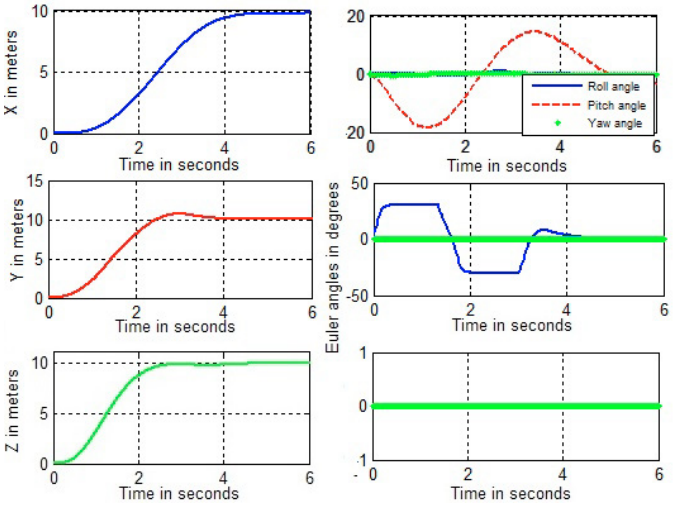

Fig. 6. Position control

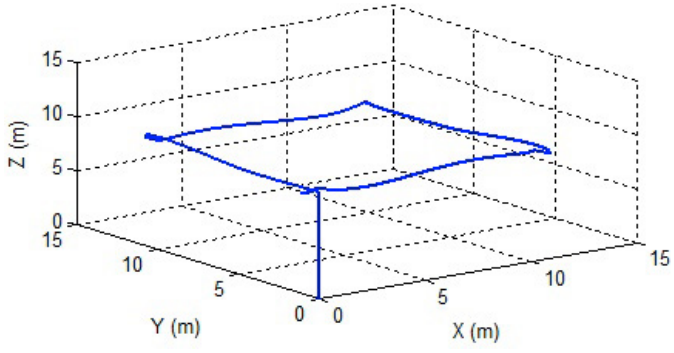

Fig. 7. Way-point tracking

Position control Position control simulation results and corresponding attitude plots for individual translation degree of freedom are shown in Fig. 6. The effect of actuator dynamics is also reflected in position control as shown in Fig. 6. As the forward motion is controlled by pitch attitude, forward translation degree of freedom is slower compared to vertical and side translation degree of freedom.

Way-point tracking We put together the translation and attitude subsystems to achieve way-point tracking. We consider a way point as desired spatial coordinates to be

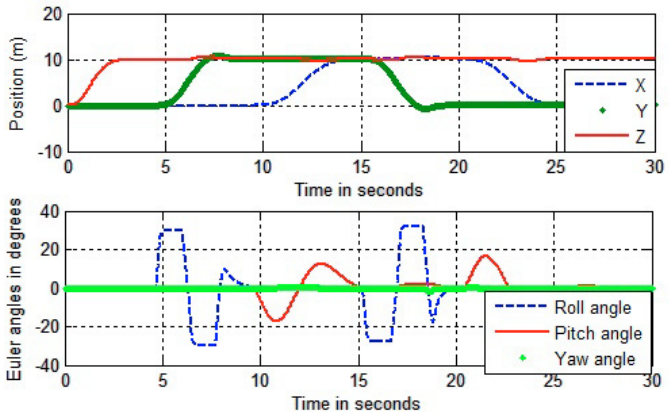

Fig. 8. Way-point tracking position and orientation plots

tracked incrementally. Once BiRW reaches the way-point then the next way point is considered as its new desired position. The way-point tracking task that we consider for BiRW is to climb 10 meters and traverse corners of a square of length 10 meters while holding altitude. We mark a way point is reached if BiRW is within some neighborhood of the way point as specified by the user. Fig.7, shows the trajectory of BiRW in spatial coordinates and the corresponding position and attitude plots are shown in Fig. 8. All the way-points are successfully tracked in approximately 25 seconds.

5. CONCLUSIONS

In this paper, we presented a novel bi-rotor configuration BiRW. A detailed modeling of forces and moments to be used in the 6-DOF model of BiRW are provided. PSO algorithm was used to compute the control gains for PD controllers for attitude and translation control so that the desired specifications are satisfied. The simulation results illustrates the efficacy of the proposed mechanism of controlling the attitude using DC motors and reaction wheels.

APPENDIX

Actuator and system parameters definitions and the numerical values of these parameters that were used in the simulations presented in this paper are given in Table 4.

Table 6. Parameters

Symbol	Definition	Value
BLDC motor parameters		
k_d	DC gain	57.6
τ_m	Time constant	0.4 s
J_m	Moment of inertia of rotor	6e-5 kgm^2
Propeller parameters		
b	Thrust constant	1.1881e-5 Ns^2
d	Counter torque constant	7e-7 Nms^2
DC motor parameters		
R_a	Armature resistance	2.7 Ω
L_a	Armature inductance	0.16 mH
k_t	Torque constant	0.9268 NmA^{-1}
k_b	Back emf constant	0.9268 Vs
J	Moment of inertia of armature	6.16e-4 kgm^2
B	Viscous friction coefficient	4.48e-5 Nms
f	Coulomb friction	7.68e-5 Nm
BiRW parameters		
m	Mass	0.832 kg
l	Arm length	0.24 m
I_x	Moment of inertia about x_b	0.0012 Kgm^2
I_y	Moment of inertia about y_b	0.0113 Kgm^2
I_z	Moment of inertia about z_b	0.0105 Kgm^2
γ_1	Angle of DC motor 1	74°
γ_2	Angle of DC motor 2	104°

REFERENCES

Bouabdallah, S., Noth, A., & Siegwart, R. PID vs LQ control techniques applied to an indoor micro quadrotor. In *Proc. of International Conference on Intelligent Robots and Systems*, Sendai, Japan, pp. 2451-2456, 2004.

Bouabdallah, S., & Siegwart, R. Full control of a quadrotor. In *Proceedings of International Conference on Intelligent Robots and Systems*, San Diego, USA, pp. 153–158, 2007.

Gupte, S., Mohandas, P. I. T., & Conrad, J. M. A survey of quadrotor unmanned aerial vehicles. In *Proceedings of IEEE Southeastcon*, Orlando, USA, pp. 1–6, 2012.

Rago, C., Prasanth, R., Mehra, R. K., & Fortenbaugh, R. Failure detection and identification and fault tolerant control using the IMM-KF with applications to the Eagle-Eye UAV. In *Proceedings of IEEE Conference on Decision and Control*, Tampa, USA, pp. 4208–4213, 1998.

Santana, V., Brandao, A. S., & Mario, S. Outdoor waypoint navigation with the AR.Drone quadrotor. In *Proceedings of International Conference on Unmanned Aircraft Systems*, Denver, USA, pp. 303–311, 2015.

Escareno, J., Salazar, S., & Lozano, R. Modeling and control of a convertible VTOL aircraft. In *Proceedings of IEEE Conference on Decision and Control*, San Diego, USA, pp. 69–74, 2006.

Farid, K., Fantoni, I., & Lozano, R. Modeling and control of a small autonomous aircraft having two tilting rotors. In *Proceedings of European Control Conference*, Seville, Spain, pp. 8144-8149, 2006.

Goncalves, F. S., et al. Small scale UAV with birotor configuration. In *Proceedings of International Conference on Unmanned Aircraft Systems*, Atlanta, USA, pp. 761–768, 2013.

Gress, G. R. Lift fans as gyroscopes for controlling compact VTOL air vehicles: overview and development status of oblique active tilting. In *Annual forum proceedings-American helicopter society*, 2007.

Christian, B., & Lanteigne, E. Pitch control of an Oblique Active Tilting bi-rotor. In *Proceedings of International Conference on Unmanned Aircraft Systems*, Orlando, USA, pp. 791–799, 2014.

Scott, D., & Pounds, P. E. Towards a more efficient quadrotor configuration. In *Proceedings of International Conference on Intelligent Robots and Systems*, Tokyo, Japan, pp. 1386–1392, 2013.

Yuhui, S., & Eberhart, R. A modified particle swarm optimizer. In *Proceedings of IEEE World Congress on Computational Intelligence*, Anchorage, USA, pp. 69–73, 1998.

Kulhare, A., Chowdhury, A. B, & Raina, G. A backstepping control strategy for the Tri-rotor UAV. In *Proceedings of Chinese Control and Decision Conference*, Taiwan, pp. 3481–3486, 2012.

Mija, S. J. Dynamic SMC control scheme with adaptively tuned PID controller for speed control of DC motor. In *Proceedings of IEEE International Conference on Industrial Technology*, Seville, Spain, pp. 187–191, 2015.